Proceedings of the ASME 2010 3rd Joint US-European Fluids Engineering Summer Meeting and 8th International Conference on Nanochannels, Microchannels, and Minichannels
FEDSM-ICNMM2010
August 1-5, 2010, Montreal, Canada

FEDSM-ICNMM2010-30462

LES OF ACTIVE SEPARATION CONTROL ON BLUFF BODIES BY STEADY BLOWING

Sándor Eichinger*
Frank Thiele
Erik Wassen
Department of Fluid Mechanics and Engineering Acoustics
Berlin Institute of Technology
Müller-Breslau-Straße 8, 10623 Berlin
Email: sandor.eichinger@cfd.tu-berlin.de

ABSTRACT

An active flow control approach was investigated in order to reduce the aerodynamic drag of a generic square-backed vehicle. The investigations were carried out at a Reynolds number of $Re_L = 500,000$*. Large Eddy Simulations were performed which are suitable for time dependent flows around vehicles with large coherent structures. After the base flow simulations active flow control was applied in order to achieve drag reduction using steady blowing through small slits near the edges of the rear surface. The blowing velocity was equal to the inflow velocity (*$v_{blow} = U_0$*), and the blowing angle was changed from* $\theta = 0^\circ$ *to* $\theta = 60^\circ$*. It is shown that these control techniques can achieve a maximum drag decrease for the* $\theta = 45^\circ$ *control version of around 12%. Additionally the effect of moving floor was studied and comparison was made for the baseline and for the* 45° *flow control variant. It was found that the stagnation point on the rear surface moves upwards, and the vertical extension of the wake section reduces, so the evolving pressure level on the back surface increases. Finally a study of the blowing velocity was performed, changing* $v_{blow} = 0.25U_0$ *until* $v_{blow} = 2.25U_0$ *at* $\theta = 45^\circ$ *blowing angle. An efficiency optimum was found around* $v_{blow} = 1.25U_0$*.*

NOMENCLATURE

B	Width of the vehicle model, m
p	Local pressure, N/m^2
c_B	Coefficient of pressure drag of the base, –
p_0	Reference pressure at inflow, N/m^2
c_D	Total drag coefficient, –
R	Radius of the rounded front, m
c_F	Coefficient of friction drag, –
Re_L	Reynolds number, based on length, –
c_H	Coefficient of pressure drag of the head, –
U_0	Inflow velocity, m/s
c_p	Local pressure coefficient, –
x,y,z	Cartesian coordinates, m
c_S	Coefficient of pressure drag of the slant, –
ν	Kinematic viscosity, m^2/s
F_D	Total drag force, N
ρ	Density, kg/m^3
H	Height of the vehicle model, m
φ	Slant angle of the vehicle, $^\circ$
h	Distance from the floor, m
L	Length of the vehicle model, m
b	Width of one actuation slit, m
c_μ	Momentum coefficient of the actuation, –
v_{blow}	Blowing velocity, m/s
$\dot{m}_{blow}$	Mass flow of the blowing slits, kg/s
P_{blow}	Power of the blowing fluid, W

*Address all correspondence to this author.

Copyright © 2010 by ASME

INTRODUCTION

Drag reduction by separation control is one focus of vehicle aerodynamics research. Dealing with vehicle aerodynamics usually means flows around bluff bodies, which are dominated by large structures with three-dimensionality and strong time-dependence. Therefore, measurements and simulations are both extremely challenging problems.

The aerodynamic forces are becoming more relevant as transportation efficiency increases due to the recent ecolonomically driven requirements. The optimization of transportation costs are leading to fuel consumption reduction, enhanced safety requirements, reduced green-house gas emissions, etc. Fuel costs can be reduced for instance by means of drag reduction. Safety issues are also strongly related to the aerodynamic forces. For bluff bodies these forces are mainly determined by the resulting pressure field and less significantly by the shear stresses. The structures inside the wake flow and around the body therefore have a great influence on the overall drag, lift, and side forces. The goal of the presented work is to find an efficient way to influence this pressure distribution so that the aerodynamic drag is reduced.

Several model-based approaches were introduced in the past in order to simplify the given problems. Morel [1] and later Ahmed et al. [2] proposed a body shape which emphasizes the characteristics of ground vehicle flows. They studied the relationship between the shape and the aerodynamic drag. They found that wake topology strongly depends on the rear slant angle. Ahmed showed that for angles larger than 30° the flow separates on the edge of the slant, and no reattachment occurs. The drag value reaches its maximum around a slant angle of 30°, and it remains relatively constant with lower values at larger angles.

One special case is the slant angle 90° or 0°. Most trucks and busses have such square-back end geometry. This paper concentrates on this model shape.

The manipulation of the mentioned structures is not a novelty, as some work has already been reported. For instance, Cooper [3,4] studied the influence of the front-edge rounding and the rear-edge shaping on the aerodynamic coefficients for a very similar bluff body shape. Also the influence of gap seals, side skirts, boat-tails, and their combination was shown for a simplified truck. These so called passive devices are capable of reducing the drag by 38% compared to the baseline configuration. The influence of the boat tail deflector angle and length on the aerodynamic drag was investigated as well. An other investigation of similar square-back shaped body was made by Balkanyi [5] et al. The purpose of this work was to investigate passive flow control devices, and as one part, the base flow without any manipulation was described as well. Reynolds number dependence of the rear-end pressure distribution was also analyzed, and they found no variation in region of $Re_H = 0.8 - 1.7 * 10^5$.

Flow manipulation with active devices has been investigated intensively in the recent years. The technological advances make it possible to energize the flow in practical instances with reasonable efficiency. The advantage of such flow control techniques is that they are easily adjustable for off-design conditions, for example side wind conditions. Numerous experimental and numerical studies have been performed on the Ahmed body mostly with fast-back geometries. Krajnović and Davidson [6, 7] performed Large Eddy Simulation (LES) on an Ahmed car with slant angles of 25° and 35° and showed that LES is capable to predict separated flows with sufficient accuracy. They gave a detailed analysis of the flow and made comparison to measurements. Wassen et al. [8–12] made extensive investigations of various active flow control approaches over slanted passenger-like bodies, including constant blowing, suction, and periodic excitation as well. Their simulation technique was also LES. Rouméas [13] et al. studied a square-back geometry with steady blowing devices along the rear edges of the model. They performed Lattice-Boltzmann simulations and calculated the drag reduction for several blowing angles. They found 29% of drag reduction with 45° blowing angle and a blowing velocity of 1.5 times the inflow velocity. The control setup used in the presented paper is similar to theirs, but the blowing slits are smaller and the simulation technique is LES.

The paper is organized as follows: first the setup for the numerical simulations is given, and in the next chapter the flow without control is described. Subsequently the used flow control approaches and the corresponding results are given.

NUMERICAL SETUP

In the present study the flow around the simplified vehicle is unsteady, three dimensional and incompressible. The governing LES equations for the spatially filtered incompressible Navier-Stokes system are:

$$\frac{\partial \bar{u}_i}{\partial x_i} = 0 \tag{1}$$

$$\frac{\partial \bar{u}_i}{\partial t} + \bar{u}_j \frac{\partial \bar{u}_i}{\partial x_j} = -\frac{1}{\rho}\frac{\partial \bar{p}}{\partial x_i} + \frac{\partial}{\partial x_j}\left(\nu \frac{\partial \bar{u}_i}{\partial x_j}\right) + \frac{1}{\rho}\frac{\partial \tau_{ij}}{\partial x_j} \tag{2}$$

where $\bar{u}_i$ and $\bar{p}$ are the filtered velocity and pressure. Since the grid itself is functioning as the filter the unresolved stresses have to be modeled. The influence of these small scales on the flow are given by the sub-grid scale stress (SGS) tensor, $\tau_{ij} = \bar{u}_i\bar{u}_j - u_i\bar{u}_j$ in equation(2). Considering the standard model of Smagorinsky, one can write:

$$\tau_{ij} = -2\nu_{SGS}\bar{S_{ij}} \tag{3}$$

Copyright © 2010 by ASME

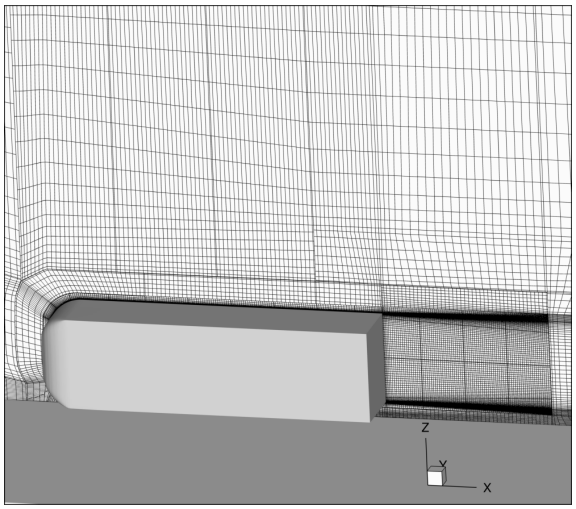

FIGURE 1. NUMERICAL GRID IN THE SYMMETRY PLANE, EVERY SECOND GRID POINT IS SHOWN.

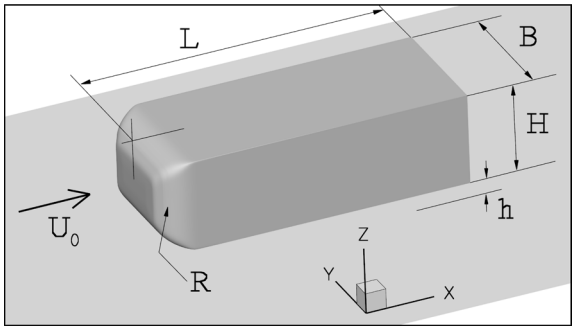

FIGURE 2. GEOMETRY OF THE AHMED BODY.

where $\bar{S_{ij}}$ is the strain rate tensor and ν_{SGS} is sub grid scale viscosity. The Smagorinsky model [14] defines ν_{SGS} as:

$$\nu_{SGS} = (C_s\Delta)^2\sqrt{2\bar{S}_{ij}\bar{S}_{ij}} \tag{4}$$

The model constant is $C_s = 0.1$, and $\Delta = \sqrt[3]{\Delta V_{ijk}}$ based on grid cell volume. For the walls van Driest [15] damping was used. The solution algorithm is of second order accuracy in space and time, the pressure is coupled with the SIMPLE method. The numerical grid in the symmetry plane is shown in figure 1. It consists of about 25 million cells, and local grid refinement is used near the body surface and in the wake region.

The size and geometry of the vehicle investigated here are identical to the original model introduced by Ahmed et al. [2]. The model, coordinate system, and the sizes are shown in figure 2. It has a height of $H/L = 0.276$, a width of $B/L = 0.373$, a distance from the floor of $h/L = 0.048$, and a radius of the rounded front of $R/L = 0.096$. The center of the coordinate system is located on the floor in the lateral symmetry plane in the level of the vertical rear-base of the body.

The computational domain is similar to a simplified wind tunnel setup with cuboid geometry. There is an upstream distance of $2.014L$ and a downstream distance of $5.793L$ behind the body to have no disturbance from the outlet of the domain. The top surface is located at $1.341L$, the side walls have a distance of $1.791L$.

At the inflow boundary a constant velocity U_0 was prescribed. On the lateral sides and on the top surface of the domain, a symmetry condition was used. It is important to note here that normally it is not recommended to use symmetry boundary conditions in LES due to the fact that is smooths down the turbulence fluctuations, but in the present case the turbulence is only generated near the walls and inside the wake. The walls of the vehicle are treated as non-slip smooth walls, likewise the floor. In case of the non-stationary floor simulation a velocity of U_0 is imposed on it.

The Reynolds number was $Re_L = U_0L/\nu = 500,000$, where ν the kinematic viscosity of the fluid. Even though the Reynolds number of a real passenger car is more than one order of magnitude higher and the drag still has a slight Reynolds number dependence, it is appropriate to study the flow at this lower Reynolds number. The reason is that the wake topology of this vehicle is fairly independent of the Reynolds number [5] since the separation at the rear end is geometry-induced.

REFERENCE FLOW

The flow topology without flow control is described in this chapter. The aerodynamic drag for these type of flows is dominated by the pressure distributions on the front and rear surfaces. The investigated bluff body has rounded edges in the front and 90° sharp edges at the rear side. As a consequence, more influential flow manipulation is expected in the wake area where the blowing slots are located. Therefore, this analysis focuses on the near wake flow.

Two reference flow cases were computed, one with stationary ground, and one with moving ground relative to the body, which is more similar to realistic road conditions. The floor movement has minor effect on the resulting forces (see table 1, and also on the corresponding wake structure.

In figure 3 projected streamlines of the time averaged flow are shown. The upper part of the figure corresponds to the vertical symmetry plane $y/H = 0$ in the near wake. The lower figure shows streamlines from the horizontal symmetry plane of the body $z/H = 0.684$. The main structure appears to be a coherent ring vortex. *Fu*, *Fb* are the foci of the upper and bottom vortical structures, respectively, *Fr* and *Fl* are the cores of two sides. The upper part of the rotating flow has a larger room, while the lower

Copyright © 2010 by ASME

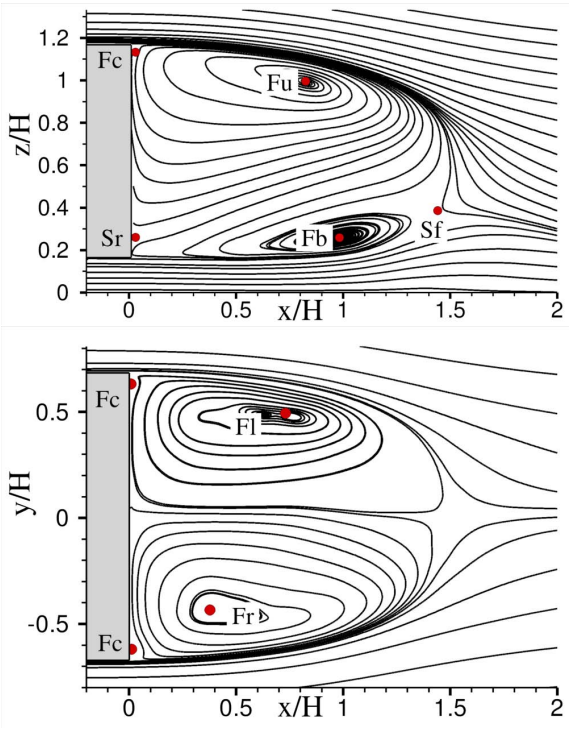

FIGURE 3. STREAMLINES OF THE TIME-AVERAGED REFERENCE FLOW; UP: SYMMETRY PLANE Y/H=0, DOWN: HORIZONTAL SYMMETRY PLANE Z/H=0.684.

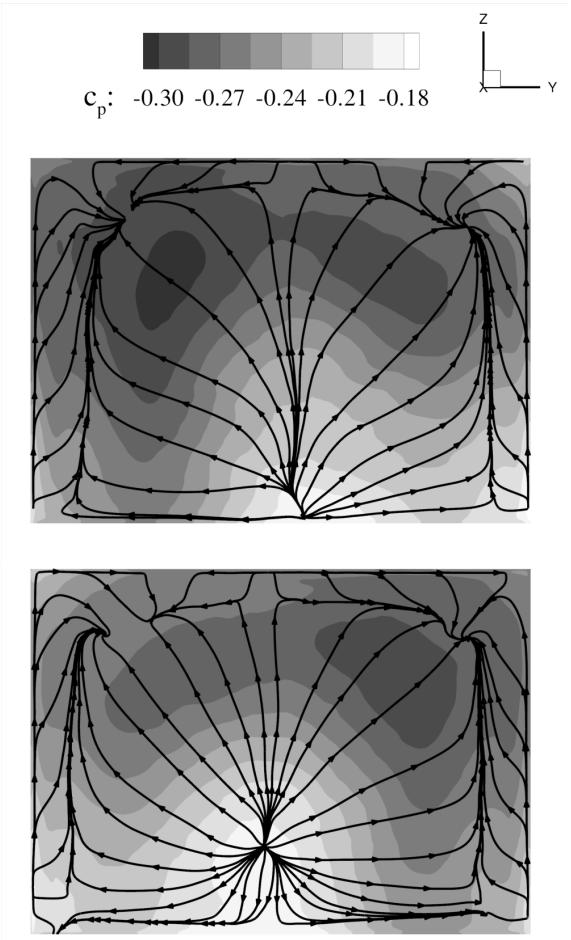

FIGURE 4. PROJECTED STREAMLINES OF THE TIME-AVERAGED FLOW ON THE VERTICAL BASE; UP: FIXED FLOOR, DOWN: MOVING FLOOR.

part is suppressed due to the boundary layer on the ground. In the case of moving floor the lower part of the ring vortex is extended in the vertical direction pushing upwards the reverse flow in the middle of the ring. If the time interval of averaging is sufficiently large the flow shows symmetry with respect to the symmetry plane $y/H = 0$, although low frequency lateral fluctuations were observed within the recirculation zone in the time dependent simulation. This makes the simulations expensive in terms of CPU time. In this instance relatively long time intervals (20 convective units) were used, however some asymmetry is still present.

Figure 4 is the image of the projected streamlines onto the rear base together with the pressure coefficient contours. The upper figure corresponds to the fixed floor, the bottom one to the moving floor. In case of moving floor due to the ground movement the outcoming underbody flow has a slightly smaller deceleration which pushes the streamwise position of the bottom part of the ring vortex *Fb* slightly downstream, and the vortex itself has a larger extension as well. Therefore the reverse flow in the case of moving floor around the middle of the recirculation zone points more upwards resulting in a higher stagnation point position *Sr* on the rear base. In the proximity of this *Sr* point the base pressure is higher indicated with light colour contour areas. Further details of the wake topology can be concluded with the help of this figure. As the reversed flow hits the wall it turns towards the 90° edges indicated with the streamlines forming the mentioned ring shape. At certain positions, where the bifurcation line is, a secondary vortex is generated. The foci of these secondary structures are indicated with *Fc* in figure 3 as well. Since the resulting drag depends mostly on the base pressure distribution, it is desirable to have more light areas on the base. The low pressure areas are located in the upper region of the base. In figure 4 it appears that the higher the stagnation point position is the lower is the contribution of the rear surface pressure to the overall aerodynamic drag.

During the simulation the total drag force is computed as the sum of the streamwise component of the pressure and friction forces over the whole bluff body at every time step. Subsequently

Copyright © 2010 by ASME

TABLE 1. CONTRIBUTION OF THE BODY PARTS TO OVERALL DRAG.

Ground treatment	C_B	C_H	C_F	C_D
Fixed	0.261	-0.017	0.035	0.279
Moving	0.251	-0.017	0.035	0.269

the time average of this value is computed, and considered as the actual aerodynamical drag force F_D. The drag coefficient c_D is computed as:

$$c_D = \frac{F_D}{\frac{1}{2}\rho {U_0}^2 BH} \tag{5}$$

In table 1 the individual components of the aerodynamic drag coefficient are shown. The value of the base drag is lower for the moving floor case which is obviously due to the higher average pressure. The drag value integrated over the head part has a negative sign. This refers to a laminar separation which takes place around the head curvature. After the laminar separation turbulent reattachment occurs. The reason is the relatively low Reynolds number ($Re_L = 500,000$). This phenomenon may influence the overall drag value, but not the wake structure, since the separation on the rear edges are clearly driven by the geometry. This assumption is also supported by the fact that the values of the head and the friction drag are identical for both ground treatment, showing no upstream - downstream influences.

CONTROL APPROACH

To achieve flow control, continuous steady blowing along the edges of the rear surface was applied as it is outlined in figure 5. Angle θ is defined between the direction of the blowing and the streamwise (or inlet) flow direction. The slits have a width of $b/H = 0.0017$, and they are positioned from the edges in the distance of b.

The basic idea was to get the drag reduction emulating the effect of passive devices like boat tails (see [3, 4]), and also to perform a study of the angle θ and the blowing intensity, similar to [13]. In the present work the investigated angles were 0°, 20°, 45°, 60°. The optimum angle was found to be 45° (see following chapters), therefore the blowing intensity was varied from $v_{blow} = 0.25U_0$ to $2.5U_0$ at this angle with the steps of $0.25U_0$, where U_0 is the inflow velocity. The corresponding momentum coefficients can be computed as follows:

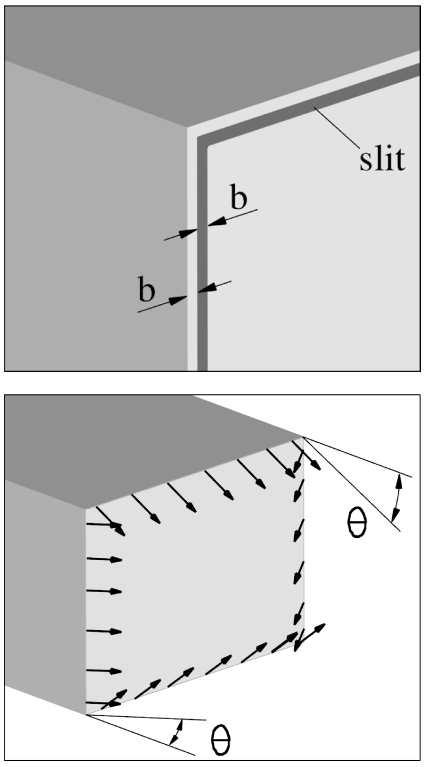

FIGURE 5. BLOWING SLITS.

$$c_\mu = \frac{2b(B+H-6b)}{BH}\left(\frac{v_{blow}}{U_0}\right)^2 cos\theta \tag{6}$$

FLOW CONTROL RESULTS

The evolution of the aerodynamic drag coefficient as a function of the blowing angle θ is shown in figure 6. The study was performed with a blowing velocity of U_0 (equal to the inflow velocity). The reference solutions are indicated with lines (solid and dashed) within the figure. As it was mentioned the highest drag decrement of 11.1 % was found at $\theta = 45°$. Blowing in the streamwise direction already results in a drag decrement of 3 %. Increasing θ up to 20° brings further decrement of 6.9 %. A larger blowing angle $\theta = 60°$, despite the 10.4 % drag improvement, shows already the tendency that further θ increment does not deliver more drag reduction. This was found by Rouméas [13] as well.

The drag differences between the control setups are only related to the pressure differences on the rear base. The friction losses and the drag on the head remain fairly constant. The upstream influence is minor which is in contrast to the experiences of the slanted Ahmed body (see [8–12]).

Copyright © 2010 by ASME

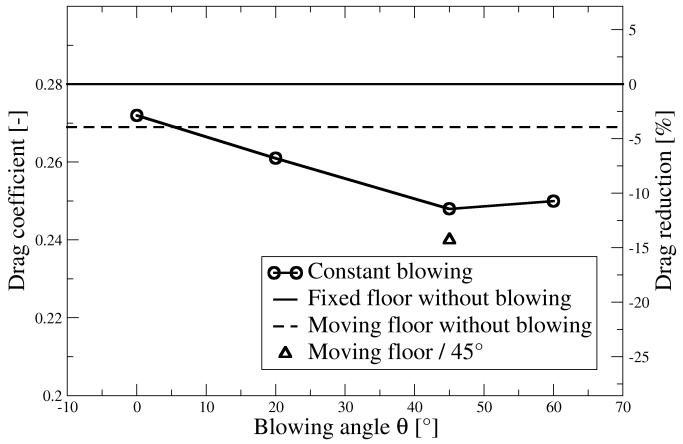

FIGURE 6. VARIATION OF BLOWING ANGLE FOR $v_{blow} = U_0$.

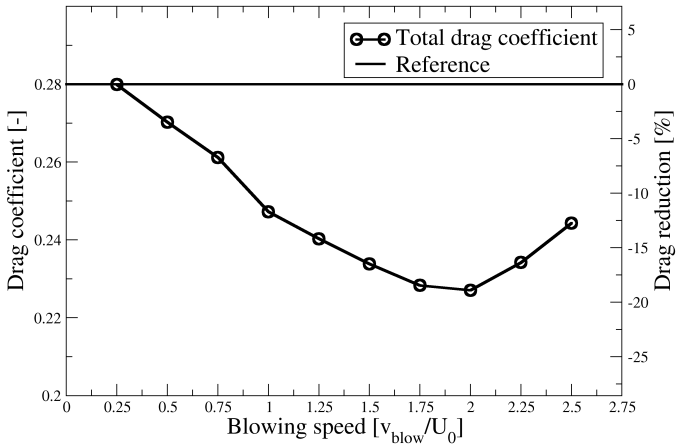

FIGURE 7. VARIATION OF BLOWING VELOCITY AT $\theta = 45°$.

After this study, the setup with $\theta = 45°$ was investigated in more detail. At first, the setup was tested with moving ground condition, which resulted in a lower drag than the controlled stationary ground case. The drag reduction compared to the reference flow (moving floor) is about 10.8 %.

Secondly, this blowing angle was used to perform a variation of the blowing speed. The aerodynamic drag results are shown in figure 7. At a very low blowing velocity, $v_{blow} = 0.25U_0$, the actuation has no influence on the drag. Increased blowing speed up to $v_{blow} = 2.0U_0$ results in increasing drag reduction up to 18.6%. Further increment of the blowing velocity leads to higher drag values.

In order to understand how the flow manipulation works, some flow topological consideration is given. In figure 8 the averaged streamlines are shown in the symmetry planes for blowing angle of $\theta = 45°$ and blowing velocity of $v_{blow} = U_0$. The main structure is the ring vortex similar to the reference flow. Indicated with the foci Fu, Fb, Fl, Fr, and the secondary vortex with Fc. Looking at the free stream stagnation point Sf, the length of the recirculation zone appears to be slightly smaller than in the baseline case. The vertical position of this point is located higher since the lower part of the ring vortex became more extensive. This effect was observed in the case of moving floor as well. Additionally the vertical extension of the wake section appears to be reduced due to the larger inclination of the streamlines near the rear-end surface, where the actuation is. Consequently, the stagnation point Sr on the rear surface is located in a higher position as in the reference flow.

Looking at the horizontal plane $z/H = 0.684$ (figure 8, bottom) one can see a significant asymmetry, although the time interval for the averaging was sufficiently large (20 CTU). The same effect can be seen in the the projected streamlines onto the rear surface of the body in figure 9. The location of the stagnation point is shifted to the right. The high pressure areas are in its proximity as well. The low pressure region on the left hand side has a moderate value compared to the reference flow case. Both effects simultaneously cause the actual drag reduction, since the integrated pressure on the rear surface is smaller. The vortex indicated with Fr has a larger extension than Fl, and the secondary vortex Fc is present along the left (looking from behind) and the upper edges. Along the right edge it is very small or rather not exists. The influence of the blowing slits can be seen as well, since there are additional bifurcation lines very close to the edges, which indicate a tertiary vortices near the jet.

The found asymmetry is not well understood, but already experienced. Blum [16] mentioned in his dissertation work that for annular jets with a high blockage ratio for various Reynolds numbers there is a symmetry breaking mechanism which results in significant asymmetry with respect to the main axis. In the present case some analogy might be present. The constant blowing through the small slits, despite the rectangular shape, might be viewed as a quasi-annular jet with very high blockage ratio. According to Blum's measurements the breakup mechanism starts with a trigger of any disturbance of the jet. In the present study the actuation was gradually switched on in a certain moment of the time-dependent flow. As mentioned above a low frequency lateral wake movement was found. When the blowing is on, this flow asymmetry interacts with the jet and, as a result, the near-wake flow "freezes" in its present state.

In order to confirm this, two test cases were simulated, us-

Copyright © 2010 by ASME

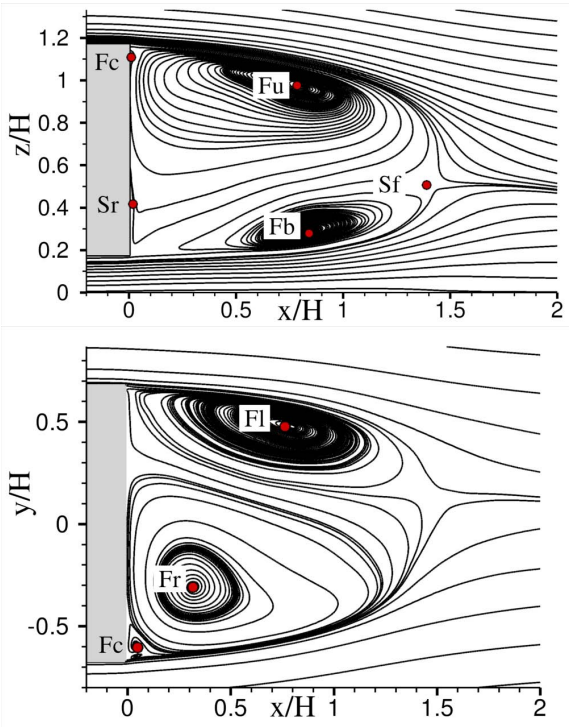

FIGURE 8. STREAMLINES OF THE TIME-AVERAGED CONTROLLED FLOW $\theta = 45°$, $v_{blow} = U_0$, STATIONARY GROUND; UP: SYMMETRY PLANE Y/H=0, DOWN: HORIZONTAL SYMMETRY PLANE Z/H=0.684.

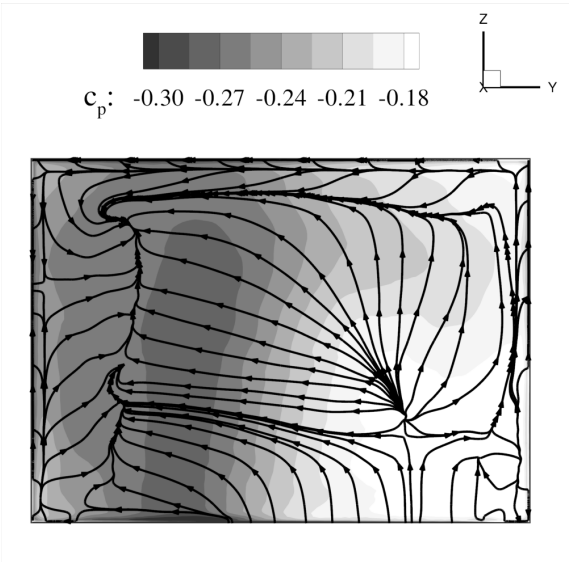

FIGURE 9. PROJECTED STREAMLINES OF THE TIME-AVERAGED FLOW ON THE VERTICAL BASE $\theta = 45°$, $v_{blow} = U_0$.

ing identical control setups ($\theta = 0°$ at U_0) but starting from different initial flow conditions. In figure 10 (top), the same initial condition was used as for the whole blowing angle and blowing intensity study. This results an asymmetry which is very similar to the one seen in figure 8 for the optimum control case, that *Fr* is more extended, and the stagnation point is somewhere on the right side of the rear surface. The bottom of figure 10 belongs to another initial instantaneous state where the wake was just flapping on the other side when the blowing was turned on. The average streamlines show that the solution "freezes" in a different position. The vortex *Fr* appears to be the smaller, and the stagnation point is located on the left side of the rear base.

EFFICIENCY

Developing an active flow control method requires an efficient system from the energy balance point of view. The energy used to generate the control must be less than the energy saved by the aerodynamic drag reduction. In order to assess the efficiency of the approach, a simple estimation is done in the following.

The propulsion power to overcome the aerodynamic drag for the reference flow is:

$$P_D = F_D U_0 = \frac{1}{2} c_D \rho B H {U_0}^3 \tag{7}$$

the energy used for the control is:

$$P_{blow} = \frac{1}{2} \dot{m}_{blow} {v_{blow}}^2 = \frac{1}{2} \rho 2b(B+H-6b) cos\theta {v_{blow}}^3 \tag{8}$$

and the energy balance is:

$$\frac{\Delta P_{net}}{P_D} = \frac{\Delta c_D}{c_{D,ref}} + \frac{P_{blow}}{P_D} \tag{9}$$

The control case is considered to be efficient when the energy balance, i.e. the sum of the additional power input due to the actuation and the power reduction due to the reduced aerodynamic drag, is negative, which means less energy input is needed. In table 2 an overview is given of the momentum coefficients, the relative power input and the power balance for all the flow control variants. The used energy for the control varies between 0.02% and 27.2% of the uncontrolled reference case. The slot geometry was same for all the control variants, this variation therefore is due to the blowing angle and blowing velocities.

It can be also seen that the power balance for almost all the cases is negative, indicating that the control technique is efficient.

Copyright © 2010 by ASME

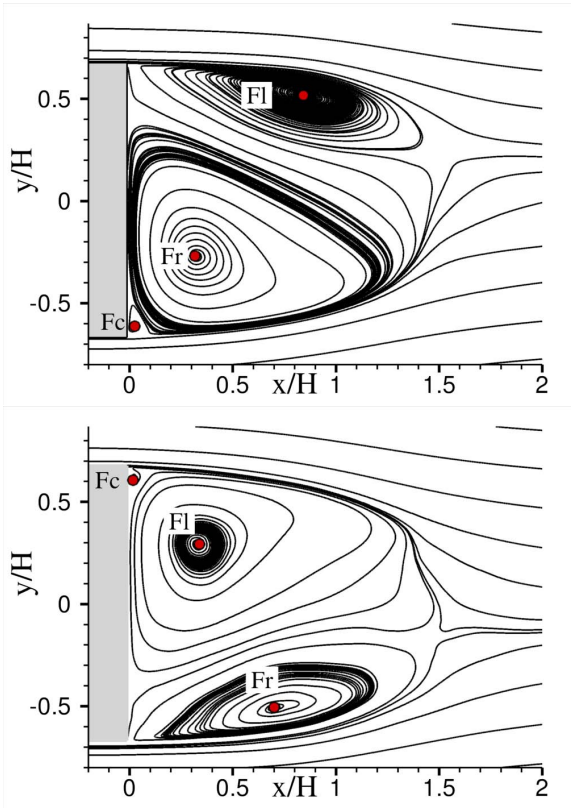

FIGURE 10. STREAMLINES OF THE TIME-AVERAGED CONTROLLED FLOW $\theta = 0°$, $v_{blow} = U_0$, FROM HORIZONTAL SYMMETRY PLANE Z/H=0.684; UP: INITIAL SOLUTION 1, DOWN: INITIAL SOLUTION 2.

The most efficient flow control variation appears to be somewhere near the blowing velocity of $1.25U_0$ at a blowing angle $\theta = 45°$. One can conclude that the best drag reduction (see figure 7) does not overlap with most efficient setup. At higher actuation intensities the drag is reduced more but the energy balance is not following this tendency. The case with very low blowing velocity $v_{blow} = 0.25U_0$ has a positive energy balance. At this low actuation intensity the drag reduction is close to zero, consequently the energy input is wasted. At very high blowing intensities, $v_{blow} = 2.25U_0$ and $v_{blow} = 2.5U_0$, the energy input is larger that the actual drag reduction, therefore the control technique is not efficient anymore.

CONCLUSIONS

Active drag reduction for a generic square-back vehicle was investigated using LES. The control method used was steady blowing along the edges of the rear surface of the model. Firstly, the blowing angle was varied from $\theta = 0°$ until $\theta = 60°$, and a maximum drag reduction of 11.1% was found at $\theta = 45°$. The drag decrement is due to the reduced integrated pressure level on the rear base caused by the wake flow deformation, as the stagnation point on the rear-end moves upwards and as the level of the minimum pressure increases. It was also observed that the application of the steady blowing stabilizes the wake in a way that can result in a largely asymmetric time-averaged wake structure. Secondly, the motion of the floor for the blowing angle with the greatest drag reduction was investigated, and it was found that the drag reduction is relatively independent of the floor movement, since almost the same drag difference was experienced as for the uncontrolled reference cases. Finally, at $\theta = 45°$ blowing angle a blowing speed variation study was performed. A maximum drag reduction of 18.6% was achieved at $v_{blow} = 2.0U_0$, while the most efficient case was found to be $v_{blow} = 1.25U_0$.

TABLE 2. MOMENTUM COEFFICIENT, RELATIVE ACTUATION POWER, AND POWER BALANCE.

Floor	v_{blow}/U_0	θ	c_μ	P_{blow}/P_D	power balance
	1	0°	0.006	2.2%	-0.7%
	1	20°	0.0057	2.2%	-4.6%
	1	45°	0.0043	1.7%	-9.4%
	1	60°	0.003	1.2%	-9.2%
	0.25	45°	0.0003	0.0%	0.4%
	0.5	45°	0.0011	0.2%	-2.9%
Fixed	0.75	45°	0.0024	0.7%	-5.7%
	1.25	45°	0.0066	3.5%	-10.4%
	1.5	45°	0.0096	6.1%	-10.0%
	1.75	45°	0.013	10.0%	-8.2%
	2.0	45°	0.017	15.0%	-3.6%
	2.25	45°	0.0215	20.7%	4.6%
	2.5	45°	0.0266	27.2%	14.8%
Moving	1	45°	0.0043	1.8%	-9.0%

ACKNOWLEDGMENT

This research was funded by the German Science Foundation (DFG) within the scope of the Collaborative Research Center SFB 557. The simulations were performed on the SGI Altix supercomputer at the North German Cooperation for High-Performance Computing (HLRN). The authors are also grate-

Copyright © 2010 by ASME

ful to Sinisa Krajnovic Chalmers University, Gothenburg, Sweden, who provided a geometry and topology of a numerical grid, which was the basis for the grid used in this study.

REFERENCES

[1] Morel, T., 1978. "The Effect of Base Slant on the Flow Pattern and Drag of Three-Dimensional Bodies with Blunt Ends". Proc. of Symp. Aerod. Drag Mechanisms of Bluff Bodies and Road Vehicles, Plenum Press, New York, pp. 191-226.

[2] Ahmed, S.R., Ramm, G., and Faltin, G., 1984. "Some salient features of the time-averaged ground vehicle wake". SAE Technical Paper Series, No. 840300.

[3] Cooper, K.R., 1985. "The Effect of Front-Edge Rounding and Rear-Edge Shaping on the Aerodynamic Drag of Bluff Vehicles in Ground Proximity". SAE Paper, 850-288.

[4] Cooper, K.R., 2003. "Truck Aerodynamics Reborn - Lessons from the Past". SAE Paper, 2003-01-3376.

[5] Balkany, Sz.R., Bernal, L.P., Khalighi, B., Sumantran, V., 2000. "Dynamics of manipulated bluff body wakes". Fluids 2000, Denver, AIAA-2000-2556.

[6] Krajnović, S. and Davidson, L., 2005. "Flow around a simplified car, Part I: Large eddy simulation". *J. Fluid Engrg.*, 127, pp. 907-918.

[7] Krajnović, S. and Davidson, L., 2005. "Flow around a simplified car, Part II: Understanding the flow". *J. Fluid Engrg.*, 127, pp. 919-928.

[8] Wassen, E. and Thiele, F., 2007. "LES of wake control for a generic fastback vehicle". AIAA Paper, 2007-4504.

[9] Brunn, A., Wassen, E., Sperber, D., Nitsche, W. and Thiele, F., 2007. "Active drag control for a generic car model". Springer, pp. 247-259, King, R. (ed.), *Active Flow Control, Notes on Numerical Fluid Mechanics and Multidisciplinary Design 95*.

[10] Wassen, E. and Thiele, F., 2008. "Drag reduction for a generic car model using steady blowing". AIAA Paper, 2008-3771.

[11] Wassen, E. and Thiele, F., 2009. "Road vehicle drag reduction by combined steady blowing and suction". AIAA Paper, 2009-4174.

[12] Wassen, E. and Thiele, F., 2010. "Simulation of active separation control on a generic vehicle". AIAA Paper, 2010-4702.

[13] Rouméas, M. Gilliéron, P. and Kourta, 2009. "Analysis of control of the near-wake flow over a square-back geometry". *Computers & Fluids*, 38, pp. 60-70.

[14] Smagorinsky, J., 1963. "General circulation experiments with the primitive equations". *Monthly Weather Review*, Vol. 91, pp. 99-164.

[15] van Driest, E.R., 1956. "On the turbulent flow near wall". *Journal of Aero Sciences*, 23, 1007-1010.

[16] Blum, L., 2005. "Flow field and turbulence measurements in different non-reacting and reacting flow configurations". Doctoral dissertation, Swiss Federal Institute of Technology Zurich.

Copyright © 2010 by ASME